Versão do arquivo anexado / Version of attached file:

Versão do Editor / Published Version

Mais informações no site da editora / Further information on publisher's website:

https://pubs.rsc.org/en/content/articlelanding/2020/cp/d0cp01025a

DOI: 10.1039/d0cp01025a

Direitos autorais / Publisher's copyright statement:

PCCP

PAPER

Check for updates

Adsorption of CO_2 and CH_4 in MIL-47 investigated by the 3D-RISM molecular theory of solvation

Cristina Gavazzoni* and Munir S. Skaf ⓘ *

Metal–organic frameworks (MOFs) comprise a class of highly porous nanomaterials formed by the assembly of organic molecular templates connected by metal ions. These materials exhibit a large diversity of pore size and geometry, topology, surface area, and chemical functionality. MOFs are particularly promising materials for developing new technologies for capture and storage of greenhouse gases such as methane and carbon dioxide. Here we apply the three dimensional reference interaction site model (3D-RISM) molecular theory of solvation to study the interactions of CO_2 and CH_4 with the metal–organic material MIL-47. The 3D-RISM integral equations were solved to determine the three dimensional density correlation functions of the gas (solvent) relative to the atomic positions of the MIL-47 framework, treated as static solute sites. The computed solvent spatial distributions inside MIL-47 pores were used to identify whether or not there exist preferable binding sites and the binding free energy landscape for the gas of interest at low computational costs compared with other molecular modeling techniques, such as grand canonical Monte Carlo and molecular dynamics simulations. The 3D-RISM formalism was applied to pure CO_2, pure CH_4, and binary mixtures of these gases of various compositions under different pressure conditions. The results indicate that both gases bind very weakly to MIL-47 and that this material exhibits nearly vanishing CO_2/CH_4 selectivity. The 3D-RISM computations presented here can be extended to investigate the physical adsorption of gases on other MOFs and nanoporous materials, providing an alternative low-cost computational approach to study gas capture and storage in nanoporous materials in general and, in particular, to determine the binding free-energy landscape in these systems.

1 Introduction

Emissions of man-made chemicals, such as carbon dioxide (CO_2) and methane (CH_4), are considered the main causes for the global climate changes. CO_2 emissions increased 1.6% to 36.2 Gt (billion tonnes) in 2017 after three years of little or no emissions growth[1,2] and CH_4 emissions increased by a factor of two in the last century.[3] As a consequence, much effort has been made to develop ways of preventing greenhouse emissions, promoting carbon capture and storage, and to repurpose these gases through chemical transformations. As the main component for natural gas, methane can be readily used in power plants providing cleaner combustion processes than coal or oil. Carbon dioxide, in turn, can be used on enhanced oil recovery[4,5] and as a processing solvent in polymer applications.[6]

However, the capture and storage of these gases are only part of the challenge. In many cases the separation of two or more gases is also needed. Natural gas, for example, also contains

carbon dioxide, nitrogen, and light hydrocarbons. The presence of CO_2 is undesirable since it reduces the energy content of the natural gas and damage the pipelines due to its corrosive behavior in the presence of water. To cope with these and other challenges, many different types of materials have been studied in order to make these technologies more efficient and economically viable. Polyethylenimine (PEI)-modified mesoporous molecular sieve of MCM-41 type, for instance, exhibits an adsorption capacity of 15 mg CO_2 per g-PEI[7] and carbon nanotube-reinforced polymeric membranes achieved a selectivity of CO_2/CH_4 ratio of up to 45.[8] Computer simulations of a porous carbon nanotube membrane indicated a high CO_2 selectivity over CH_4 due to size exclusion,[9] identified high CH_4 storage capacity in carbon-based materials,[10] and were used to screen several zeolites in terms of CO_2 selectivity.[11]

Metal–organic framework (MOFs) materials have been widely studied due to their promising technological applications in several areas,[12,13] in particular, gas separation, purification, and storage due to the fact that their structure and properties can be easily tuned to the molecular level. MOFs are constructed by linking inorganic secondary building units with organic linkers and, by combining different units, one can

Institute of Chemistry and Center for Computing in Engineering and Sciences, University of Campinas – Unicamp, Campinas, SP, 13082-864, Brazil. E-mail: crisgava@gmail.com, skaf@unicamp.br

design a MOF with the desired pore size, functional groups or accessible sites.[14] Several MOFs were already studied as possible adsorbents for CO_2, CH_4, and several other gases,[15–19] and, yet, the increasing number of possibilities when it comes to develop new MOFs makes the screening of an ideal material for a specific application a highly non-trivial task. Therefore, it is vital to use fast and reliable methods to characterize new materials and to identify adsorption mechanisms that may lead to improved MOF properties.

In the computational field, grand canonical Monte Carlo[20–22] (GCMC) and molecular dynamics (MD) simulations are the most commonly used techniques to study gas adsorption in MOFs, whereas quantum chemical methods are required for investigating catalysis and other reactive processes.[23–25] Using GCMC, it is possible to compute important thermodynamic equilibrium properties such as gas uptake, species selectivity, and adsorption enthalpy under different thermodynamic conditions. MD simulations, in turn, are quite suitable to study transport properties and have been applied in several studies, including methane diffusion[3] and CO_2 transport properties in MIL-47,[26] water interaction with MOF-5,[27] and benzene diffusion in MOF-5.[28] Recently, machine learning approaches have been proposed to identify MOFs with the desired properties. Machine learning methods were applied to predict CO_2 working capacity and CO_2/H_2 selectivity[29] in MOFs and in quantitative structure–property relationship models to identify high-performing MOFs for methane purification.[30]

Despite the indubitable power of GCMC and MD techniques to investigate gas adsorption thermodynamics and transport in MOFs and other nanostructured materials,[31–33] estimating local binding affinities of guest molecules at specific sites of the host nanostructured framework is challenging because the binding affinity is a measure of the host–guest binding free energy, a computationally-demanding quantity to compute by molecular simulations.[34] The 3D-RISM-KH (three dimensional reference interaction site model with the Kovalenko–Hirata closure approximation) is a molecular theory of solvation based on a first-principles statistical mechanics integral equation formalism that allows for the calculation of the ensemble-averaged, equilibrium spatial solvent distribution around a given solute molecule or host site at a much lower computational cost compared to other methods.[35] From the equilibrium spatial solvent distribution obtained by solving the integral equations, several thermodynamic properties can be calculated analytically, including binding enthalpies and, most notably, the three-dimensional (3D) host–guest binding free-energy landscape across the nanostructure. Like GCMC or MD molecular simulation methods, 3D-RISM-KH uses atomistic force fields to describe the intermolecular interactions and has been successfully applied to a variety of problems, such as the selective ion-binding by proteins,[36] adsorption of alkali ions in Prussian Blue nanoparticles,[37] the behavior of interfacial water in biological systems,[38] the structure and stability of oligomeric polyelectrolyte gel networks,[39] and the generalized binding forces in model ligno-cellulosic materials,[40,41] to name a few examples. Furthermore, combinations between simulations and the 3D-RISM were proposed in order to enhance the computation speed.[42,43]

Here we apply the 3D-RISM-KH solvation theory to study adsorption and selectivity of CO_2 and CH_4 gases by MIL-47 – a metal organic framework consisting of infinite chains of corner-sharing $V^{4+}O_6$ octahedra connected by terephthalate groups that lead to a one-dimensional diamond shaped pore. The MIL-47 structure was fully characterized by Barthelet et al.[44] and has been studied for adsorption and separation of xylene isomers and ethylbenzene,[45] hydrogen sulfide adsorption,[46] methane and CO_2 diffusion,[3,26] and CO_2 uptake.[47] Differently from the isostructural MIL-53, MIL-47 has a rigid, breathing-free structure,[47] which is ideal for 3D-RISM calculations,[35] since flexible structures would require performing calculations for several possible solute structures in order to understand the material behavior. For such systems, 3D-RISM techniques could also be combined with Monte Carlo or MD simulations to generate an ensemble of different structures, which may depend on the gas loading. Our goal here is to investigate binding of CO_2 and CH_4 to the MIL-47 structure and to examine CO_2/CH_4 selectivity (or lack thereof) under different external pressure conditions using the 3D-RISM-KH formalism as a test-case for 3D-RISM computation of the binding free-energy landscape in nanostructured materials. Computations were carried out for gas densities in the range 0.001–0.1 g cm^{-3}, which correspond approximately to external pressures in the range 0.5–50 bar and 1.0–140 bar for CO_2 and CH_4, respectively.

2 The 3D-RISM solvation theory

In this work we obtained the three dimensional density correlation functions by numerically solving the 3D-RISM integral equations carrying ensemble-average structural information for a system containing a solvated macromolecule.[35,48–50] An excellent review of the theory and its application to a variety of molecular systems has been provided by Fedorov and co-workers.[35] For a solute–solvent system at infinite dilution, the 3D-RISM integral equations reads

$$h_\gamma(\mathbf{r}) = \sum_\alpha \int d\mathbf{r}' c_\alpha(\mathbf{r}') \chi_{\alpha\gamma}(|\mathbf{r} - \mathbf{r}'|) \quad (1)$$

where $h_\gamma(\mathbf{r})$ and $c_\gamma(\mathbf{r})$ are the total and direct correlation functions of the γ solvent site around the solute macromolecule, respectively, and $\chi_{\alpha\gamma}(\mathbf{r})$ is the solvent–solvent pair susceptibility function. In order to calculate the solvent–solvent susceptibility function one must solve the equations for the dielectrically consistent one-dimensional RISM theory.[51] The $\chi_{\alpha\gamma}(\mathbf{r})$ is given by

$$\chi_{\alpha\gamma}(\mathbf{r}) = w_{\alpha\gamma}^{\text{solv}}(r) + \rho h_{\alpha\gamma}^{\text{solv}}(r) \quad (2)$$

where $h_{\alpha\gamma}^{\text{solv}}(r)$ is the solvent–solvent total correlation function in the absence of the solute and $w_{\alpha\gamma}^{\text{solv}}(r)$ is the intramolecular correlation function that describe the structure of the solvent molecule. Therefore, the solvent–solvent susceptibility function carries information about the solvent interactions in the absence of the solute.

In order to obtain the three dimensional correlation functions, eqn (1) must be complemented with a closure equation.

Kovalenko and Hirata[48] (KH) closure couples the mean spherical approximation (MSA) and the hypernetted chain (HNC) closure to describe strongly associative liquid systems accurately. The numerical stability of the RISM calculations under the KH approximation *versus* HNC and other closure relations has been discussed for the chemical potential of strongly attractive ionic solutions.[52] In the 3D-RISM formalism, the KH closure reads:

$$g_\gamma(\mathbf{r}) = \begin{cases} \exp\left[-u_\gamma(\mathbf{r})/(k_B T) + h_\gamma(\mathbf{r}) - c_\gamma(\mathbf{r})\right] & \text{if } g_\gamma(\mathbf{r}) \leq 1 \\ 1 - u_\gamma(\mathbf{r})/(k_B T) + h_\gamma(\mathbf{r}) - c_\gamma(\mathbf{r}) & \text{if } g_\gamma(\mathbf{r}) > 1 \end{cases} \tag{3}$$

where $g_\gamma(\mathbf{r}) = h_\gamma(\mathbf{r}) + 1$ is the normalized local solvent density distribution around solute site γ relative to the bulk distribution, also known as density correlation function, T is temperature, k_B is the Boltzmann constant and $u_\gamma(\mathbf{r})$ is the interaction potential between solvent and solute sites, usually described as a sum of Lennard-Jones and Coulomb potentials in many force fields.

Unlike MC or MD molecular simulations, 3D-RISM and other integral equation approaches usually require a soft-core repulsive potential at every charged site in order to prevent the build up of spurious solvent density fields near the origin. This may be particularly relevant for highly compressible fluids such as the ones considered here. The success of RISM-KH calculations with modified potentials obtained by adding soft-core Lennard-Jones terms on charged hydrogen atoms has been demonstrated for supercritical water under different density (0.025–1.0 g cm^{-3}) and temperature (300–800 K) conditions in the presence of self-ionization processes,[53] for density fluctuation calculations of water from vapor-like to liquid-like densities (0.0001 to 1.0 g cm^{-3}), with focus on the near critical region,[54] as well as on the liquid–vapor coexistence of water and methanol, both in bulk and sorbed in nanoporous carbon aerogel.[55] In their 2002 paper,[55] Kovalenko and Hirata provide a very nice historical account of the RISM-KH development from the liquid state theory point of view where these and other issues are discussed.

The potential of mean force (PMF) centered at particular MOF site γ provides the free energy profile for ligand binding as a function of the distance between a solvent molecule (ligand) and γ and is related to the local density correlation function $g_\gamma(\mathbf{r})$ by:

$$\text{PMF}_\gamma(\mathbf{r}) = -k_B T \ln[g_\gamma(\mathbf{r})] \tag{4}$$

The PMF is the reversible work involved in bringing two or more selected particles from infinity separation to a final configuration[56] and, in this sense, it is the Gibbs free energy difference between these two states at constant pressure and temperature. The solute–solvent adsorption or binding free energy, ΔG, is defined as $\Delta G = \text{PMF}(\mathbf{r}_{\min})$ where $\mathbf{r}_{\min}$ is the distance where the PMF reaches the minimum.

Here, the calculations were carried out for T = 300 K and several densities of the solvent gas. The Lennard-Jones (LJ) parameters and charges where taken from the TraPPE model for the CH$_4$[57] and from the EPM2 model for the CO$_2$.[58] The structure used for MIL-47 was obtained from the Barthelet *et al.* study.[44] The potential parameters for MIL-47 were taken from previous molecular simulations of CO$_2$ in MIL-47,[26] on which a LJ soft-core has been added to the vanadium atoms. The vanadium distance (σ = 3.144 Å^3) and energy (ε = 0.016 kcal mol^{-1}) parameters were taken from the UFF force field[59] without any further refinement. Fig. 1 shows a fragment of the MIL-47 structure. For the calculations, this structure was replicated 10 times along the longitudinal axis of the tube (x direction).

The 3D-RISM was solved considering a cubic supercell of 128 × 128 × 128 Å^3 divided in 128^3 grid points. The MOF was placed inside the simulation box with its center of mass coinciding with the center of the box. The dielectric constant of all the solvent gas was set to 1 and the integrals were converged to a root mean square accuracy of 1 × 10^{-4}. The 1D and 2D profiles were obtained by averaging over the area of normalization or the axis of normalization as follows

$$g(z) = \frac{\int_{\text{area}} g(\mathbf{r}) \, \mathrm{d}x \, \mathrm{d}y}{\int_{\text{area}} \mathrm{d}x \, \mathrm{d}y}, \quad \text{1D properties} \tag{5}$$

$$g(y,z) = \frac{\int_{\text{axis}} g(\mathbf{r}) \, \mathrm{d}x}{\int_{\text{axis}} \mathrm{d}x}, \quad \text{2D properties} \tag{6}$$

All calculations were performed using the RISM suite implemented in the Amber package.[60] Since the 3D-RISM-KH framework is designed for more dense liquid systems, it is
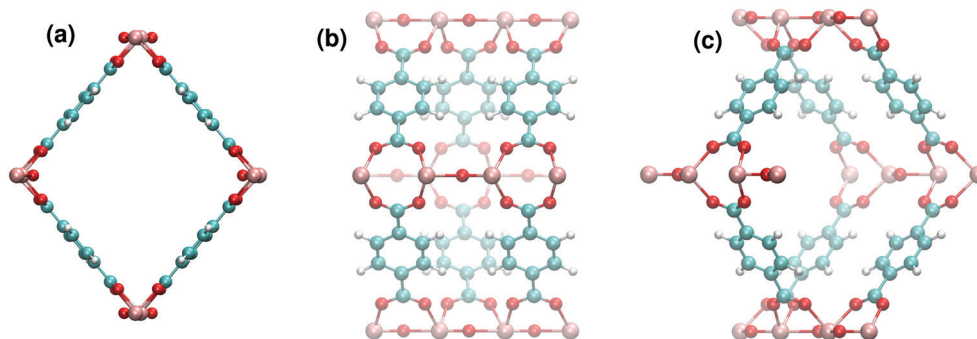
Fig. 1 MIL-47 Structure. Vanadium, oxygen, carbon, and hydrogen atoms are shown in pink, red, blue, and white, respectively. View from the (a) z–y plane, (b) x–y plane and (c) diagonal view.

13242 | *Phys. Chem. Chem. Phys.*, 2020, **22**, 13240–13247

This journal is © the Owner Societies 2020

important to ascertain that the calculations are reliable under the low density conditions considered here. Therefore, we computed the pair correlation functions for both gases in the absence of the MOF for ρ = 0.001, 0.01 and 0.1 g cm^{-3}. The $g(r)$ for carbon atoms are well behaved and present a first peak at r = 4 Å for CH$_4$ and r = 4.2 Å for CO$_2$. The peak heights are approximately 1.5 for both gases and the results for CO$_2$ are consistent with those reported by Koga *et al.*[61] for carbon dioxide under supercritical thermodynamic conditions using an HNC-like closure.

3 Results

3.1 Pure solvent

First, we study the adsorption of pure CO$_2$ and CH$_4$ in MIL-47. From the 3D–RISM calculation, we obtained a three dimensional density correlation function that shows, for each grid point, the value of the local gas density with respect to that of the bulk, *i.e.*, how many times more likely it is to find a gas molecule around that position relative to the bulk. Fig. 2 shows the two dimensional density correlation obtained by averaging the three-dimensional distribution over the longitudinal axis of the MIL-47 pores.

For lower densities, CH$_4$ exhibits a weak preference for the corners of the pore and, as the density increases, the distribution becomes even more diffuse, as depicted in the left panels of Fig. 2: for ρ = 0.001 g cm^{-3} ($\sim$1.5 bar), the regions marked red represent sites in which methane molecules are found with a probability about seven times higher than in the bulk. As the density increases, the regions marked red (high CH$_4$ concentration) become increasingly less prominent, indicating a more homogeneous occupancy of the MIL-47 pore by CH$_4$ molecules.

Methane is a relatively bulky molecule compared to the MIL-47 pore diameter, roughly spherically symmetric and
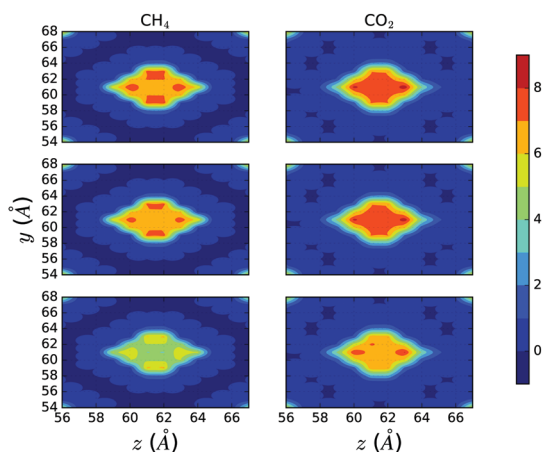
nonpolar, with zero dipole and quadrupole moments. According to our results, it shows no strong preference for any specific site along the tunnel-like pore of the framework. Therefore, the organization of the methane inside the pore is determined essentially by dispersion interactions and the packing of molecules inside the pores. Occupying the corners allows for CH$_4$ molecules to settle, while avoiding unfavorable competition among them. As the density increases, the methane is forced to fill the pore more uniformly.

Distinctively, for ρ = 0.001 g cm^{-3} ($\sim$0.56 bar), CO$_2$ molecules fill the pore almost uniformly, with densities as large as seven times the bulk density at these thermodynamic conditions (right panels in Fig. 2). Nevertheless, there is a small region in the left and right corners of the pore where the probability of finding a carbon dioxide molecule is eight times the bulk density (regions marked in dark red). As the CO$_2$ density increases, this preference for the horizontal corners of the pore becomes more apparent.

Carbon dioxide, unlike CH$_4$, has a significant quadrupole moment ($[1.427 \pm 0.061] \times 10^{-39}$ C m^2)[62] and may interact with specific sites of the MOF. For the particular case of MIL-47, a reentrant oxygen linked to two adjacent vanadium can be found on the equatorial right and left corners of the pore (see Fig. 1), creating, on both sides, a local dipole moment pointing to the center of the pore, thus providing preferable interaction sites for CO$_2$ *via* dipole–quadrupole interaction. Nevertheless, a recent study[47] suggested that, due to the relatively weak enthalpy of adsorption observed experimentally, no specific adsorption sites are expected in the MIL-47 sample for the CO$_2$ quadrupole to interact with. In order to understand this apparent discrepancy, we investigated the 2D density correlation function on the x–y plane, the 3D density correlation function and the potential of mean force (PMF). As discussed below, the specific interactions between MIL-47 and CO$_2$ seen in the calculations are indeed too small to be detected by adsorption calorimetry.

Fig. 3 shows the 2D density correlation function on the x–y plane compared with the position of the atoms in the MIL-47 structure. Methane is found nearly equally distributed along the tunnel, with no particular correlation with any MIL-47 site (top panel in Fig. 3). The CO$_2$ longitudinal distribution, on the other hand, is markedly correlated with the positions of the reentrant oxygens of MIL-47, located near positions x = 61.5, 65.5 and 69 Å in this picture.

The 3D spatial maps of density distributions $g_\gamma(\mathbf{r})$ of representative solvent sites in the interior of the nanostructure for both methane and carbon dioxide are shown in Fig. 4 for $g > 4$. The 3D maps indicate the regions inside the nanopores where the local density enhancement of carbon (blue) and oxygen (green) atoms is at least four times that of the bulk and allow reconstruction of preferred binding modes. Methane shows a mild preference to occupy the regions near the surface of the pore rather than its center, whereas carbon dioxide appears to fill the pore more uniformly, with the carbon atoms mostly at the center and oxygens further out close to the pore surface. The vertical peaks exhibited by the oxygen 3D map indicate an

Fig. 2 2D density correlation function on the z–y plane for CH$_4$. Different densities are shown: ρ = 0.001 g cm^{-3} (upper panels), ρ = 0.01 g cm^{-3} (mid panels) and ρ = 0.10 g cm^{-3} (lower panels). Red represents high probability and blue lower probability of finding a solvent molecule, relative to the bulk.

This journal is © the Owner Societies 2020

Phys. Chem. Chem. Phys., 2020, **22**, 13240–13247 | **13243**
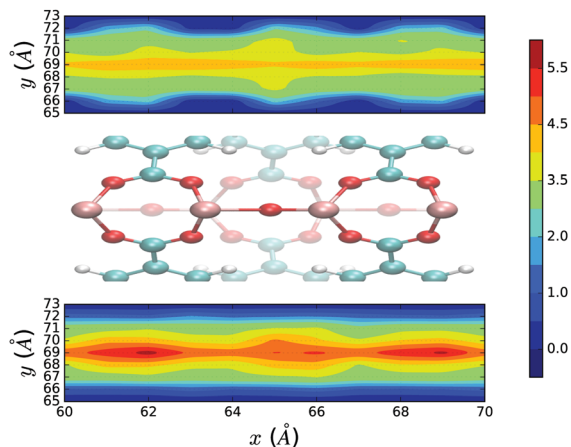
Fig. 3 2D density correlation function on the x–y plane for CH_4 (top) and CO_2 (bottom) for $\rho = 0.10$ g cm^{-3}. Red represents high probability and blue lower probability of finding a solvent molecule. For clarity, the structure of MIL-47 is shown in the middle.
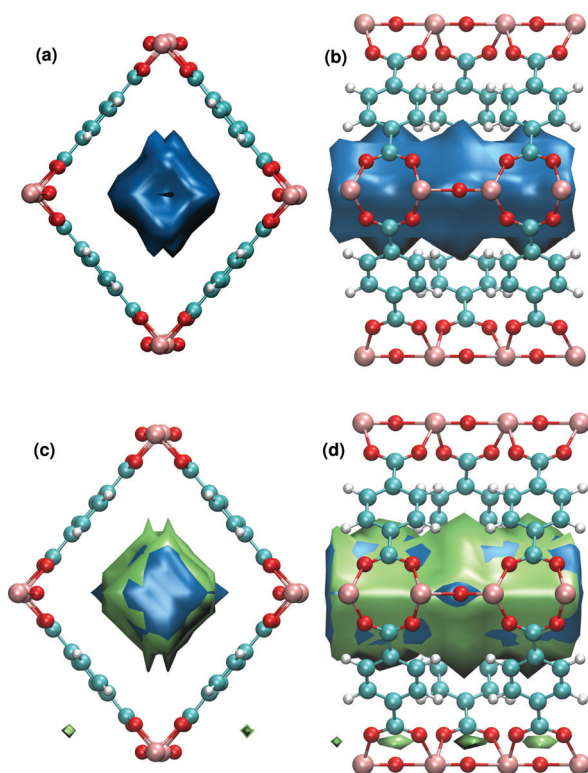
Fig. 4 3D density correlation function for CH_4 ((a) z–y plane and (b) x–y plane) and CO_2 ((c) z–y plane and (d) x–y plane) for $\rho = 0.10$ g cm^{-3}. The colors represent the carbon (blue) for both molecules and CO_2 oxygen (green). The surfaces are shown for $g > 4$.

Fig. 5 Potential of mean force in the x direction for density (a) $\rho = 0.01$ g cm^{-3} and (b) $\rho = 0.07$ g cm^{-3}.

shown in Fig. 5 for $\rho = 0.01$ and 0.07 g cm^{-3}. The oscillatory behavior seen in Fig. 5 reflects the atomic roughness of the MOF. For methane the lowest values correspond to interstitial spaces in the MOF structure, whereas for carbon dioxide the lowest minima correspond roughly to regions near the MOF's oxygen atoms. A hint of this is reflected in the small spikes seen in Fig. 4 for CO_2 (green) and can also be seen in Fig. 3, which shows periodic minima roughly 4 Å apart along the main axis for CO_2. The amplitudes of the oscillations, however, are less than 0.1 kcal mol^{-1} and are essentially immaterial to the discussion. ΔG is estimated from the average PMF over the extension $40 < x < 90$ Å.
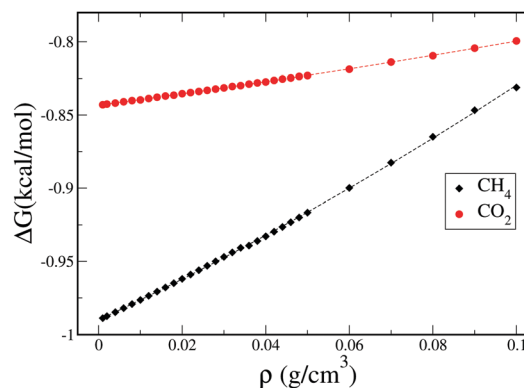
Fig. 6 ΔG_{ads} for CH_4 and CO_2 as a function of density.

organization of carbon dioxide molecules aligned to the y-axis of the MOF, consistent to the slipped parallel structure,[63] and the T-like dipole–quadrupole interactions.

The PMF profile is related to the solvent distribution function by means of eqn (3), from which the Gibbs binding free energy, ΔG, for each species can be computed, as discussed above. The computed PMF along the principal axis of MIL-47 is

13244 | *Phys. Chem. Chem. Phys.*, 2020, **22**, 13240–13247

This journal is © the Owner Societies 2020

Fig. 6 shows ΔG as a function of the bulk gas density for both CH_4 (black) and CO_2 (red). Methane turns out slightly more stable than carbon dioxide inside the nanostructure, which, in turn, is less affected by increasing the gas density or pressure. Methane adsorption is slightly more sensitive to the available volume and, therefore, increasing the density affects the ability of MIL-47 to capture CH_4. However, the difference in ΔG between the two gases is very small compared to thermal energy, varying from approximately 0.15 kcal mol^{-1} at ρ = 0.001 g cm^{-3} to 0.06 kcal mol^{-1} at ρ = 0.10 g cm^{-3}, indicating that MIL-47 is not CH_4/CO_2 selective. Moreover, this small difference in the free energy suggest that, despite of the existence of mildly preferred position near the reentrant oxygen,

the quadrupolar interactions of the CO_2 with this particular site is not significant for the adsorption process.

3.2 Mixtures

Let us now consider the molecular distribution inside the MIL-47 structure for CO_2–CH_4 mixtures. Calculations were made for several total densities and compositions. Fig. 7 shows the 2D density correlation function for different molar fractions (x_{CH_4} = 0.1, 0.5, and 0.9) at ρ_{total} = 0.01 and 0.07 g cm^{-3}. Methane behaves similarly for all total densities studied: for low x_{CH_4} there is a relatively large region with high probability of finding a methane molecule (seven and six times more likely then the bulk for ρ_{total} = 0.01 and 0.07 g cm^{-3}, respectively). As the methane molar fraction increases, this region shrinks. The 2D density correlation functions for CO_2 show a stretching of the CO_2 distribution in the z direction for all mixtures
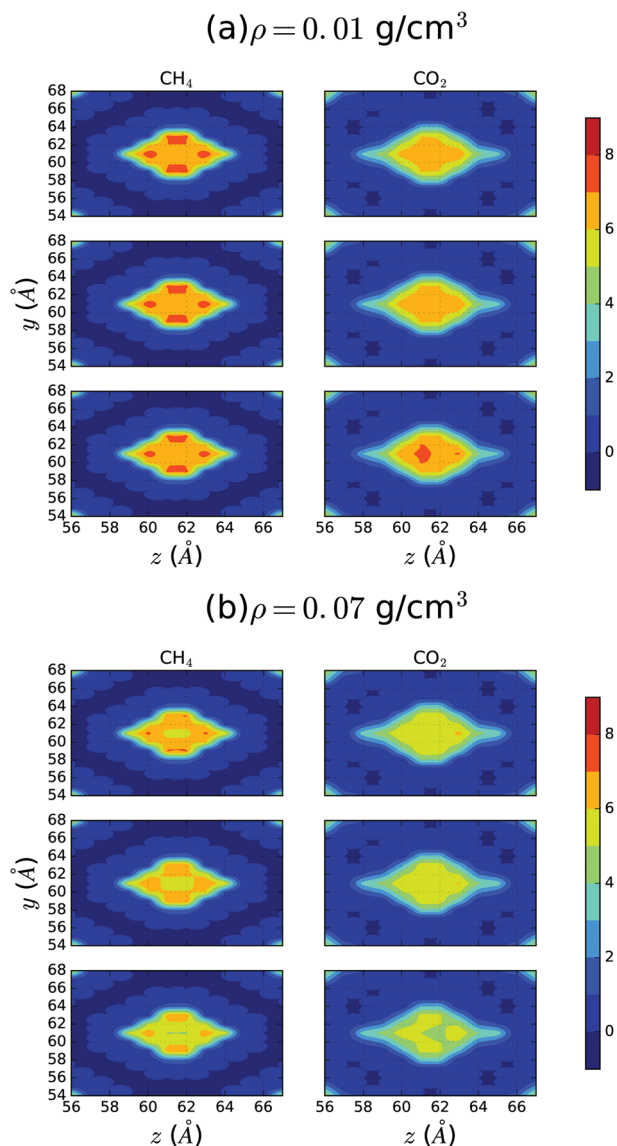
Fig. 7 2D density correlation function on the z–y plane for CH_4 and CO_2 for (a) ρ_{total} = 0.01 g cm^{-3} and (b) ρ_{total} = 0.07 g cm^{-3}. Results for different molar fractions are shown: x_{CH_4} = 0.1 (top panels), x_{CH_4} = 0.5 (mid panels) and x_{CH_4} = 0.9 (lower panels). Red represents high probability and blue lower probability of finding a solvent molecule.
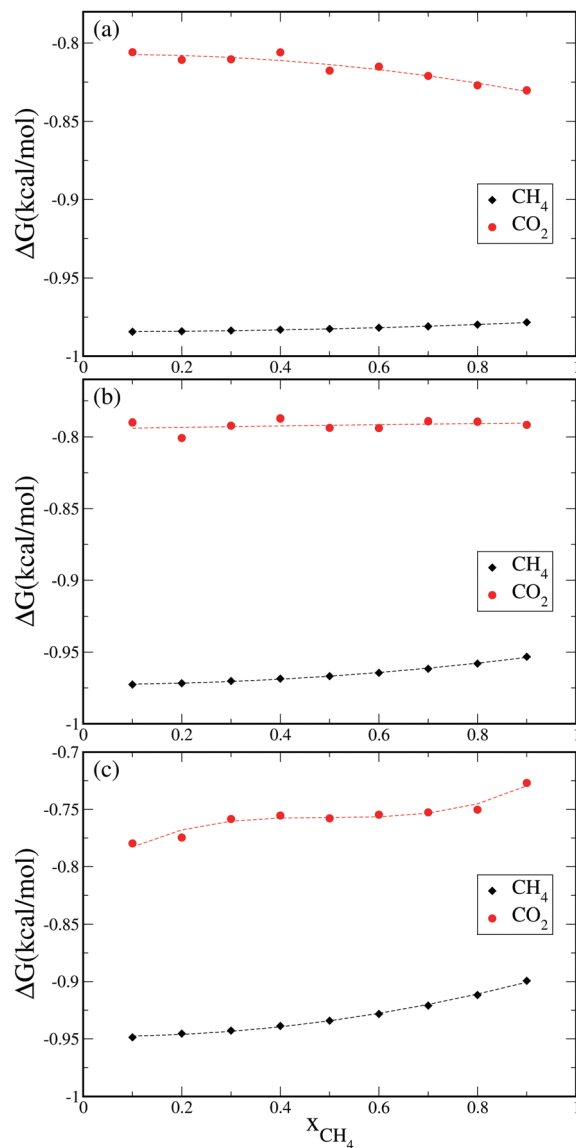
Fig. 8 ΔG_{ads} for CH_4 and CO_2 as a function of methane molar fraction for (a) ρ = 0.01 g cm^{-3}, (b) ρ = 0.03 g cm^{-3} (c) ρ = 0.07 g cm^{-3}.

considered and CO_2 molecules become restricted to the center of the tunnel-like pore, a region slightly unpreferred by CH_4.

The computed binding free energy of each species is shown in Fig. 8 as function of the composition for ρ = 0.01, 0.03, and 0.07 g cm^{-3}. The binding of these gases to MIL-47 is quite insensitive to composition, with methane binding slightly better when mixed with carbon dioxide than when present as pure solvent. At lower (higher) total bulk density, CO_2 molecules tend to increase (decrease) its binding affinity as the mixture gets richer in methane. That is, depending on the bulk density, the trend of the CO_2 binding to MIL-47 with composition may change. The small CH_4 over CO_2 selectivity may become even smaller at low total density for CH_4-rich mixtures (Fig. 8a). Nevertheless, this effect seems to be way too small for any practical purposes.

4 Concluding remarks

In this work, we applied the 3D-RISM integral equation formalism to study the molecular distribution and binding free-energy of CH_4, CO_2 and CH_4/CO_2 mixtures in the metal–organic material MIL-47. Calculations were carried out for T = 300 K, different bulk densities, and several molar fractions in the case of mixtures. From the 3D-RISM theory we obtained a three dimensional density correlation function, which allows the identification of preferred interactions sites, and the computation Gibbs free-energy profile obtained from the potential of mean force.

We studied the adsorption of the CH_4 and CO_2 separately and identified two different adsorption mechanisms. Methane adsorption is simply due to the packing of molecules inside the pore, whereas carbon dioxide also interact with the reentrant oxygen atoms linked to two adjacent vanadium sites on the equatorial right and left corners of the pore *via* a dipole–quadrupole coupling. This additional interaction, however, is not strong enough to effectively influence the gas adsorption and, as a consequence, does not provide the energetic advantage needed for separation of CO_2. Therefore, despite of the high CO_2 uptake reported,[47] the MIL-47 metal–organic material would not exhibit CO_2/CH_4 selectivity according to our calculations.

We showed that the 3D-RISM formalism used in this work is an effective tool to determinate adsorption sites, adsorption free energies and to make propositions on the adsorption mechanisms and selectivity in MOFs. It has the advantages of being dielectrically consistent, in the thermodynamic limit by definition, fast and economically viable which makes this technique a reliable way to study small molecules dispersion on nanostructured materials such as MOFs. Whereas 3D-RISM method provides an attractive approach to compute adsorption free-energy landscapes for such a system, the computation of total gas uptake *via* 3D-RISM is not as straightforward because it would require a nontrivial spatial integration of the density distribution. However, since gas uptake can be readily calculated by means of GCMC simulations, 3D-RISM methods can be combined with GCMC techniques using the same force fields to gain a more detailed understanding of gas adsorption on MOFs.

Conflicts of interest

There are no conflicts to declare.

Acknowledgements

References

1 R. B. Jackson, C. Le Quéré, R. M. Andrew, J. G. Canadell, J. I. Korsbakken, Z. Liu, G. P. Peters and B. Zheng, *Environ. Res. Lett.*, 2018, **13**, 120401.

2 R. B. Jackson, C. Le Quéré, R. M. Andrew, J. G. Canadell, G. P. Peters, J. Roy and L. Wu, *Environ. Res. Lett.*, 2017, **12**, 110202.

3 N. Rosenbach Jr, H. Jobic, A. Ghoufi, F. Salles, G. Maurin, S. Bourrelly, P. L. Llewellyn, T. Devic, C. Serre and G. Férey, *Angew. Chem., Int. Ed.*, 2008, **47**, 6611–6615.

4 M. L. Godec, V. A. Kuuskraa and P. Dipietro, *Energy Fuels*, 2013, **27**, 4183–4189.

5 V. Alvarado and E. Manrique, *Energies*, 2010, **3**, 1529–1575.

6 S. P. Nalawade, F. Picchioni and L. P. B. M. Janssen, *Prog. Polym. Sci.*, 2006, **31**, 19–43.

7 X. Xu, C. Song, J. M. Andresen, B. G. Miller and A. W. Scaroni, *Energy Fuels*, 2002, **16**, 1463–1469.

8 L. Deng and M.-B. Hägg, *Int. J. Greenhouse Gas Control*, 2014, **26**, 127–134.

9 B. J. Bucior, D.-L. Chen, J. Liu and J. K. Johnson, *J. Phys. Chem. C*, 2012, **116**, 25904–25910.

10 S. P. Collins, E. Perim, T. D. Daff, M. S. Skaf, D. S. Galvao and T. K. Woo, *J. Phys. Chem. C*, 2018, **123**, 1050–1058.

11 R. Krishna and J. Van Baten, *Chem. Eng. J.*, 2007, **133**, 121–131.

12 P. Horcajada, R. Gref, T. Baati, P. K. Allan, G. Maurin, P. Couvreur, G. Ferey, R. E. Morris and C. Serre, *Chem. Rev.*, 2011, **112**, 1232–1268.

13 A. Cadiau, J. S. Lee, D. D. Borges, P. Fabry, T. Devic, M. T. Wharmby, C. Martineau, D. Foucher, F. Taulelle and C.-H. Jun, *et al.*, *Adv. Mater.*, 2015, **27**, 4803.

14 W. Lu, Z. Wei, Z.-Y. Gu, T.-F. Liu, J. Park, J. Park, J. Tian, M. Zhang, Q. Zhang and T. Gentle III, *et al.*, *Chem. Soc. Rev.*, 2014, **43**, 5561–5593.

15 D. Saha, Z. Bao, F. Jia and S. Deng, *Environ. Sci. Technol.*, 2010, **44**, 1820–1826.

16 Y. Xiong, Y.-Z. Fan, D. D. Borges, C.-X. Chen, Z.-W. Wei, H.-P. Wang, M. Pan, J.-J. Jiang, G. Maurin and C.-Y. Su, *Chem. – Eur. J.*, 2016, **22**, 16147–16156.

17 D. D. Borges, P. Normand, A. Permiakova, R. Babarao, N. Heymans, D. S. Galvao, C. Serre, G. De Weireld and G. Maurin, *J. Phys. Chem. C*, 2017, **121**, 26822–26832.

18 H.-Y. Cho, D.-A. Yang, J. Kim, S.-Y. Jeong and W.-S. Ahn, *Catal. Today*, 2012, **185**, 35–40.

19 M. Ding, R. W. Flaig, H.-L. Jiang and O. M. Yaghi, *Chem. Soc. Rev.*, 2019, **48**, 2783–2828.

20 R. F. Cracknell, *Phys. Chem. Chem. Phys.*, 2001, **3**, 2091–2097.

21 D. D. Borges, M. Prakash, N. A. Ramsahye, P. L. Llewellyn, S. Surblé, P. Horcajada, C. Serre and G. Maurin, *Mol. Simul.*, 2015, **41**, 1357–1370.

22 D. D. Borges, R. Semino, S. Devautour-Vinot, H. Jobic, F. Paesani and G. Maurin, *Chem. Mater.*, 2017, **29**, 1569–1576.

23 J. Yu, L.-H. Xie, J.-R. Li, Y. Ma, J. M. Seminario and P. B. Balbuena, *Chem. Rev.*, 2017, **117**, 9674–9754.

24 S. Yadnum, S. Choomwattana, P. Khongpracha, J. Sirijaraensre and J. Limtrakul, *ChemPhysChem*, 2013, **14**, 923–928.

25 L.-M. Yang, P. Ravindran, P. Vajeeston, S. Svelle and M. Tilset, *Microporous Mesoporous Mater.*, 2013, **175**, 50–58.

26 F. Salles, H. Jobic, T. Devic, P. L. Llewellyn, C. Serre, G. Ferey and G. Maurin, *ACS Nano*, 2010, **4**, 143–152.

27 J. A. Greathouse and M. D. Allendorf, *J. Am. Chem. Soc.*, 2006, **128**, 10678–10679.

28 S. Amirjalayer and R. Schmid, *Microporous Mesoporous Mater.*, 2009, **125**, 90–96.

29 H. Dureckova, M. Krykunov, M. Z. Aghaji and T. K. Woo, *J. Phys. Chem. C*, 2019, **123**, 4133–4139.

30 M. Z. Aghaji, M. Fernandez, P. G. Boyd, T. D. Daff and T. K. Woo, *Eur. J. Inorg. Chem.*, 2016, 4505–4511.

31 P. Naeiji, T. K. Woo, S. Alavi, F. Varaminian and R. Ohmura, *J. Chem. Phys.*, 2019, **150**, 114703.

32 B. S. Gelfand, R. P. S. Huynh, S. P. Collins, T. K. Woo and G. K. Shimizu, *Chem. Mater.*, 2017, **29**, 10469–10477.

33 S. Nandi, P. De Luna, T. D. Daff, J. Rother, M. Liu, W. Buchanan, A. I. Hawari, T. K. Woo and R. Vaidhyanathan, *Sci. Adv.*, 2015, **1**, e1500421.

34 C. Chipot and A. Pohorille, *Free energy calculations*, Springer, 2007.

35 E. L. Ratkova, D. S. Palmer and M. V. Fedorov, *Chem. Rev.*, 2015, **115**, 6312–6356.

36 Y. Kiyota, R. Hiraoka, N. Yoshida, Y. Maruyama, T. Imai and F. Hirata, *J. Am. Chem. Soc.*, 2009, **131**, 3852–3853.

37 N. Ruankaew, N. Yoshida, Y. Watanabe, H. Nakano and S. Phongphanphanee, *Chem. Phys. Lett.*, 2017, **684**, 117–125.

38 M. C. Stumpe, N. Blinov, D. Wishart, A. Kovalenko and V. S. Pande, *J. Phys. Chem. B*, 2010, **115**, 319–328.

39 A. Kovalenko, A. E. Kobryn, S. Gusarov, O. Lyubimova, X. Liu, N. Blinov and M. Yoshida, *Soft Matter*, 2012, **8**, 1508–1520.

40 R. L. Silveira, S. R. Stoyanov, S. Gusarov, M. S. Skaf and A. Kovalenko, *J. Am. Chem. Soc.*, 2013, **135**, 19048–19051.

41 C. S. Pereira, R. L. Silveira, P. Dupree and M. S. Skaf, *Biomacromolecules*, 2017, **18**, 1311–1321.

42 S. M. Kast, *Phys. Chem. Chem. Phys.*, 2001, **3**, 5087–5092.

43 I. Omelyan and A. Kovalenko, *J. Chem. Theory Comput.*, 2015, **11**, 1875–1895.

44 K. Barthelet, J. Marrot, D. Riou and G. Férey, *Angew. Chem., Int. Ed.*, 2002, **41**, 281–284.

45 L. Alaerts, C. E. A. Kirschhock, M. Maes, M. A. Van Der Veen, V. Finsy, A. Depla, J. A. Martens, G. V. Baron, P. A. Jacobs and J. F. M. Denayer, *et al.*, *Angew. Chem., Int. Ed.*, 2007, **46**, 4293–4297.

46 L. Hamon, C. Serre, T. Devic, T. Loiseau, F. Millange, G. Férey and G. D. Weireld, *J. Am. Chem. Soc.*, 2009, **131**, 8775–8777.

47 S. Bourrelly, P. L. Llewellyn, C. Serre, F. Millange, T. Loiseau and G. Férey, *J. Am. Chem. Soc.*, 2005, **127**, 13519–13521.

48 A. Kovalenko and F. Hirata, *J. Chem. Phys.*, 1999, **110**, 10095–10112.

49 A. Kovalenko and F. Hirata, *J. Chem. Phys.*, 2000, **112**, 10391–10402.

50 A. Kovalenko, *Pure Appl. Chem.*, 2013, **85**, 159–199.

51 A. Kovalenko, *Molecular theory of solvation*, Springer, 2004, pp. 169–275.

52 S. M. Kast and T. Kloss, *J. Chem. Phys.*, 2008, **129**, 236101.

53 N. Yoshida, R. Ishizuka, H. Sato and F. Hirata, *J. Phys. Chem. B*, 2006, **110**, 8451–8458.

54 M. Matsugami, N. Yoshida and F. Hirata, *J. Chem. Phys.*, 2014, **140**, 104511.

55 A. Kovalenko and F. Hirata, *J. Theor. Comput. Chem.*, 2002, **1**, 381–406.

56 A. Ben-Naim, *Molecular theory of solutions*, Oxford University Press, 2006.

57 M. G. Martin and J. I. Siepmann, *J. Phys. Chem. B*, 1998, **102**, 2569–2577.

58 J. G. Harris and K. H. Yung, *J. Phys. Chem.*, 1995, **99**, 12021–12024.

59 A. K. Rappé, C. J. Casewit, K. S. Colwell, W. A. Goddard III and W. M. Skiff, *J. Am. Chem. Soc.*, 1992, **114**, 10024–10035.

60 T. Luchko, S. Gusarov, D. R. Roe, C. Simmerling, D. A. Case, J. Tuszynski and A. Kovalenko, *J. Chem. Theory Comput.*, 2010, **6**, 607–624.

61 K. Koga, H. Tanaka and X. C. Zang, *J. Phys. Chem.*, 1996, **100**, 16711–16719.

62 C. Graham, D. A. Imrie and R. E. Raab, *Mol. Phys.*, 1998, **93**, 49–56.

63 K. W. Jucks, Z. S. Huang, D. Dayton, R. E. Miller and W. J. Lafferty, *J. Chem. Phys.*, 1987, **86**, 4341–4346.

This journal is © the Owner Societies 2020

Phys. Chem. Chem. Phys., 2020, **22**, 13240–13247 | **13247**